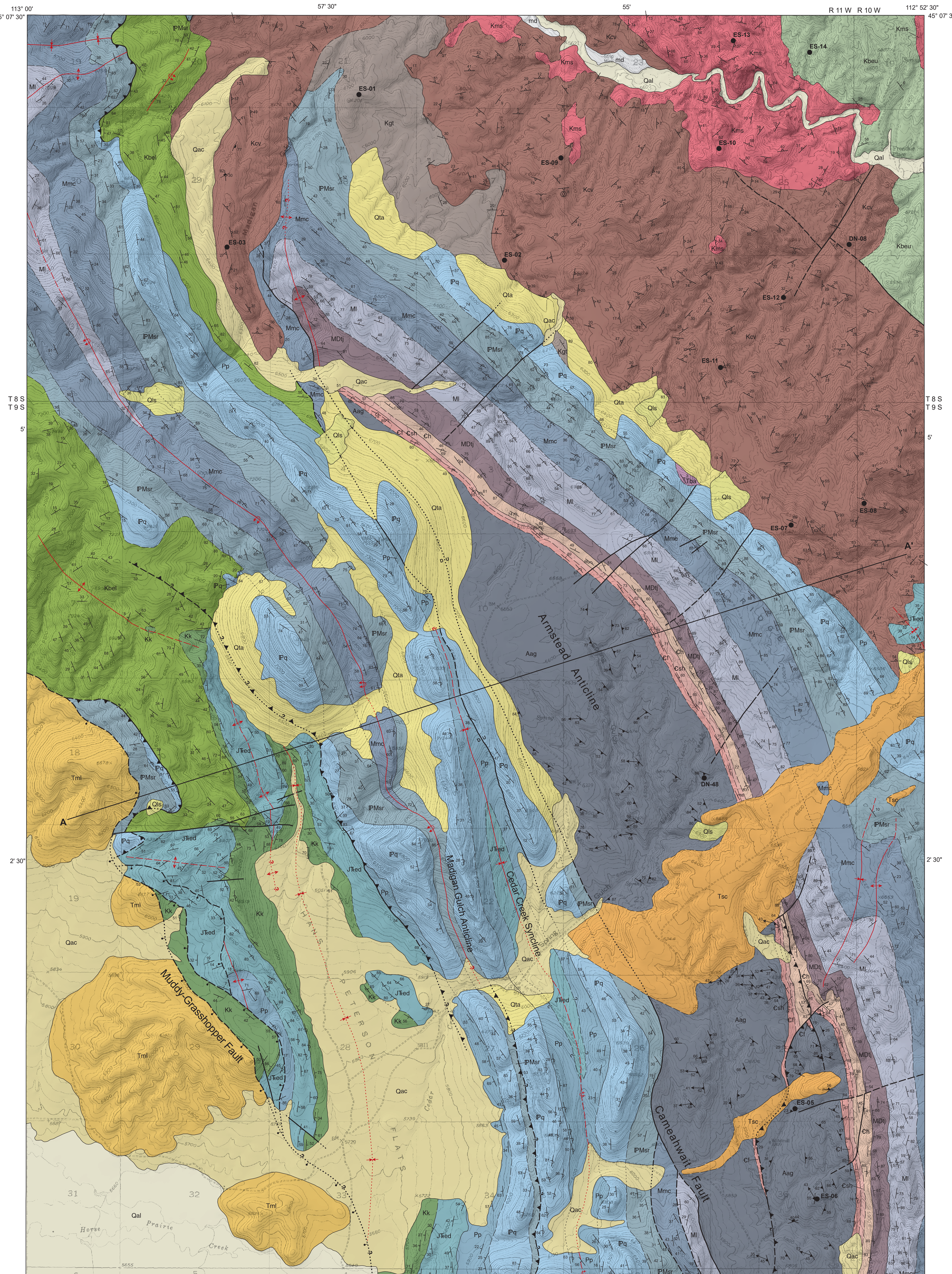

Base map produced by the United States Geological Survey
Eli Spring 1:24,000-scale topographic map
Control by: USGS, and USC&GS
Compiled from aerial photographs taken 1950
Field checked: 1952 Map photoinspected: 1976
Projection: Polyconic
Grid: 1000 meter Universal Transverse Mercator Zone 12
Vertical Datum: National Geodetic Vertical Datum of 1929
Horizontal Datum: 1927 North American Datum

Shaded-relief created from 10 meter digital elevation model from U.S. Geological Survey National Elevation Dataset.

SCALE 1:24,000

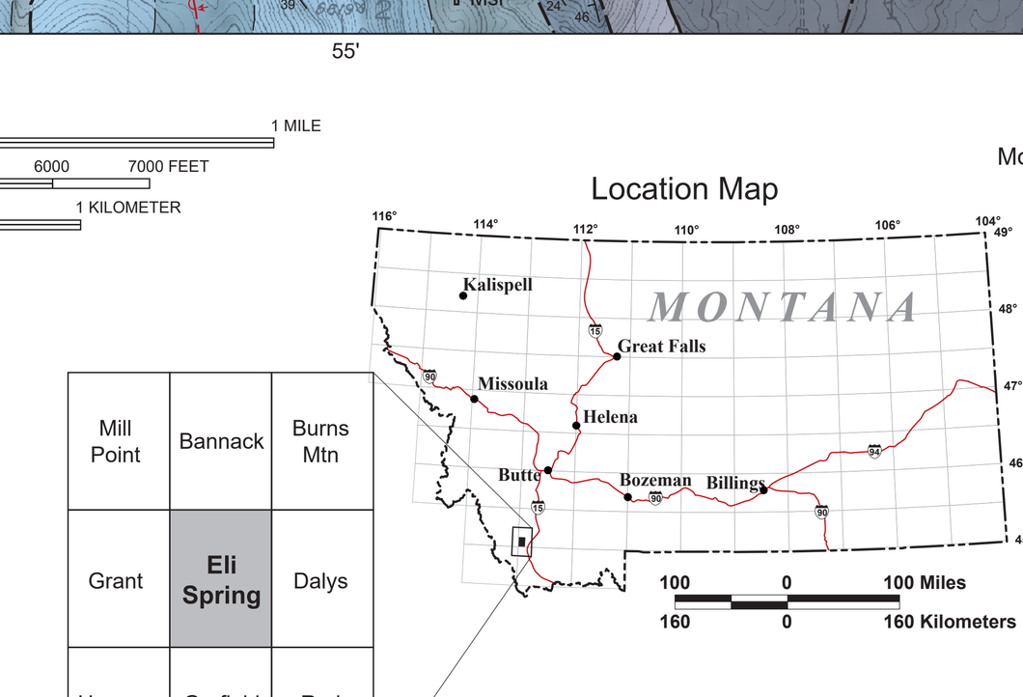

Maps may be obtained from:
Publications Office
Montana Bureau of Mines and Geology
1300 West Park Street
Butte, Montana 59701-8997
Phone: (406) 496-4174
http://mbmg.mtech.edu

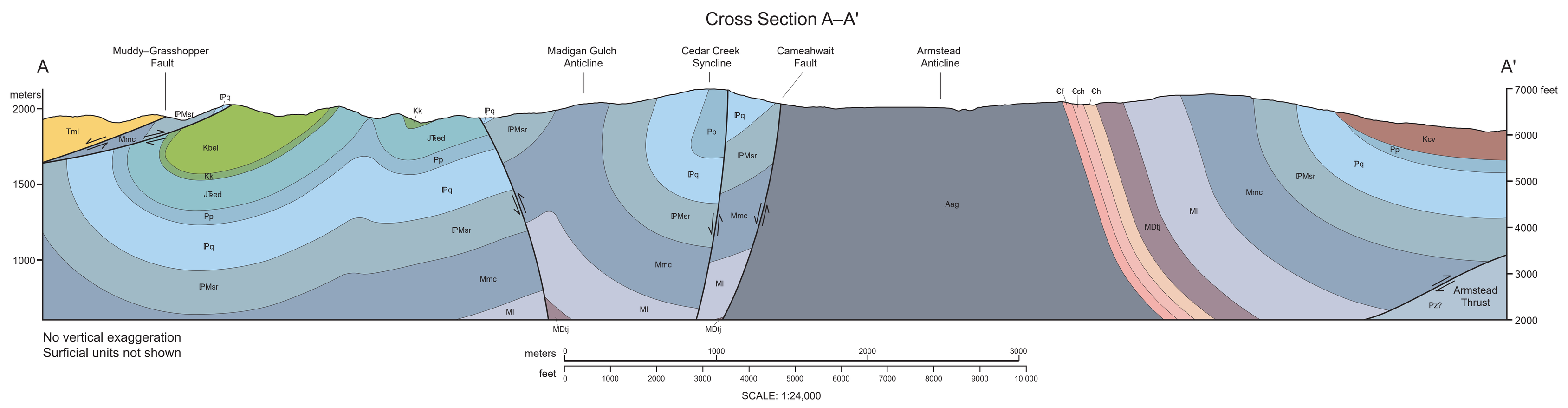

Research supported by the U.S. Geological Survey, National Cooperative Geologic Mapping Program, under USGS award G18AC00200.
GIS production: Yiwen Li and Paul Thale, MBMG. Map layout: Susan Smith, MBMG. Editing: Susan Barth, MBMG.

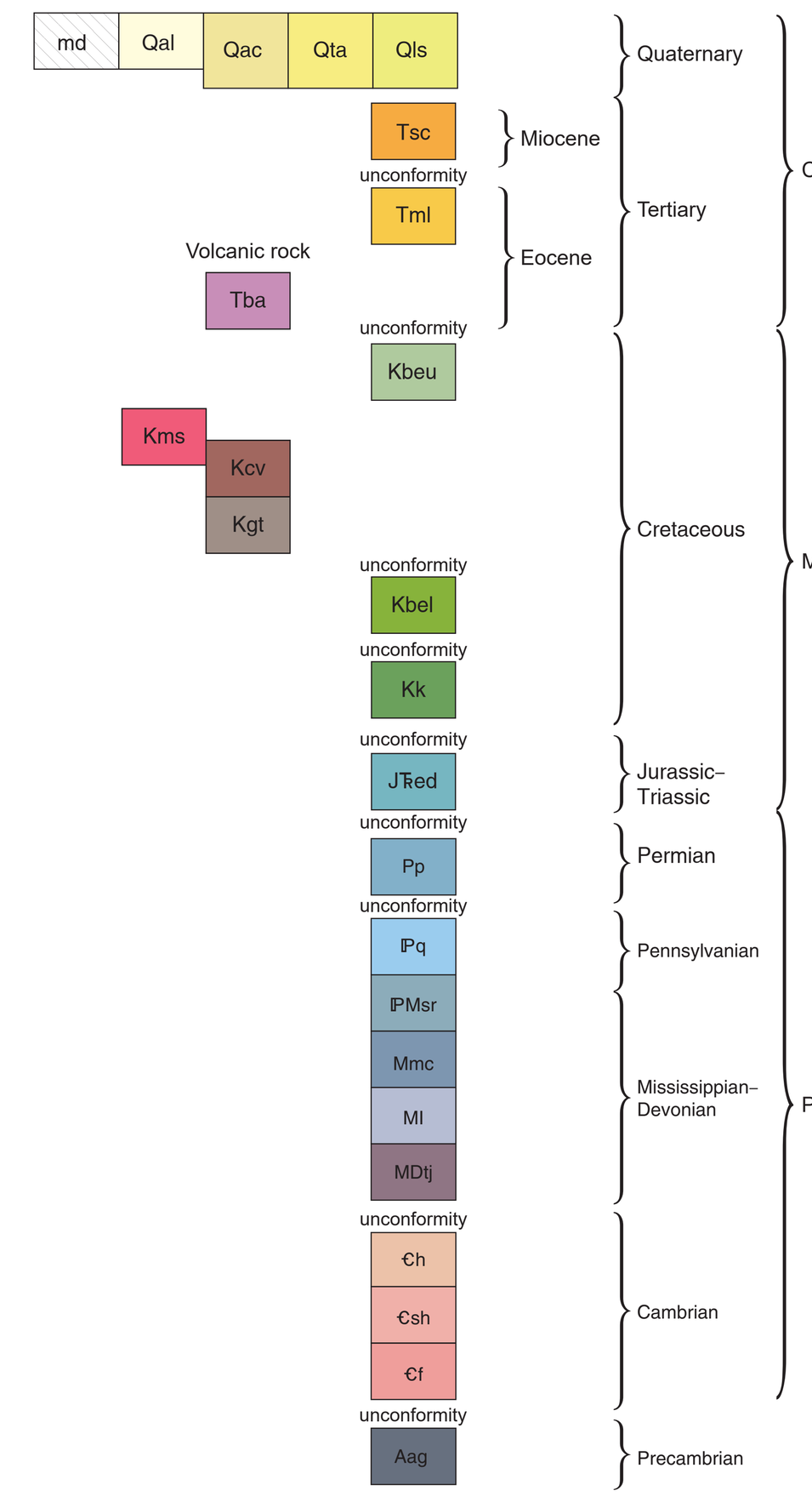

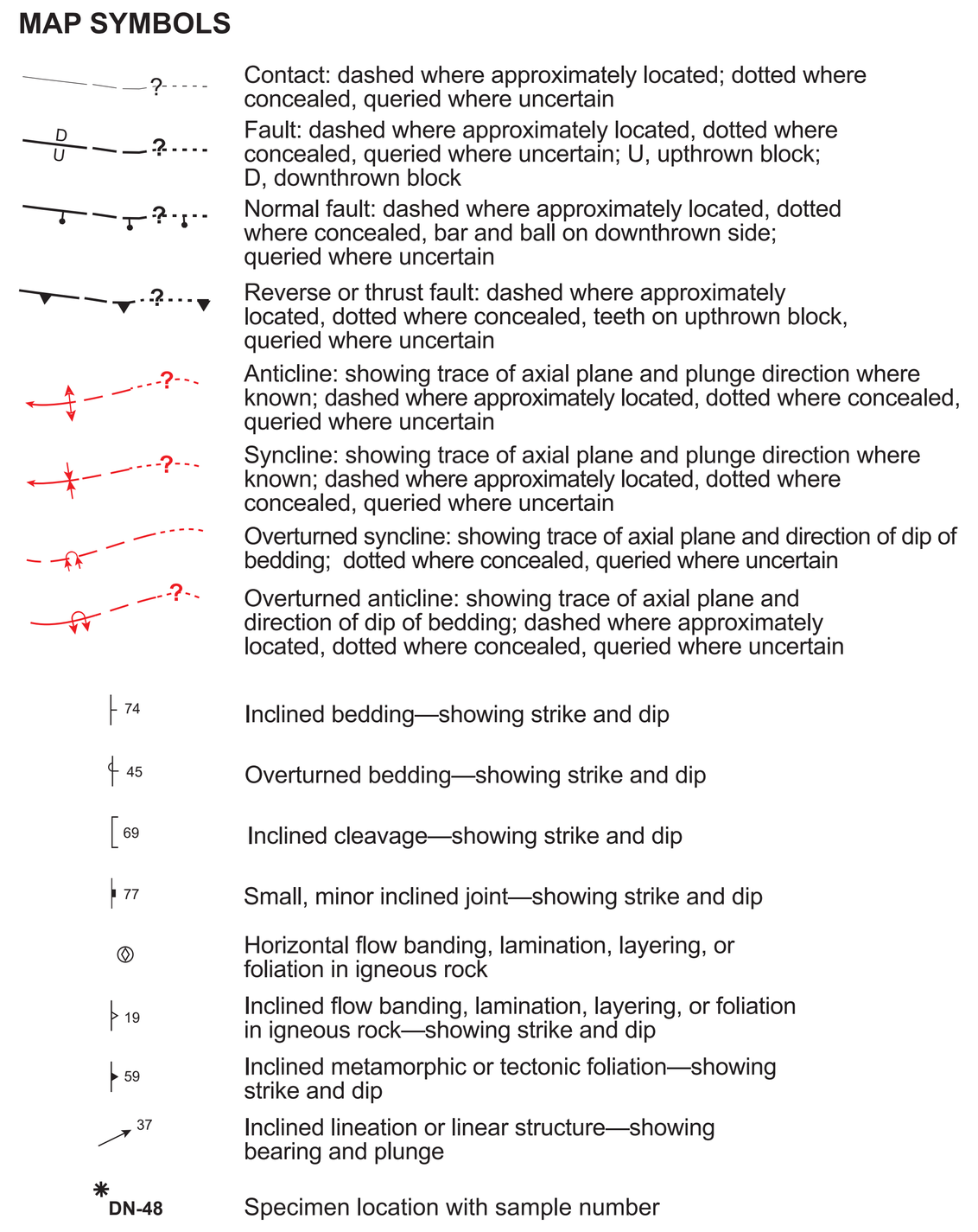

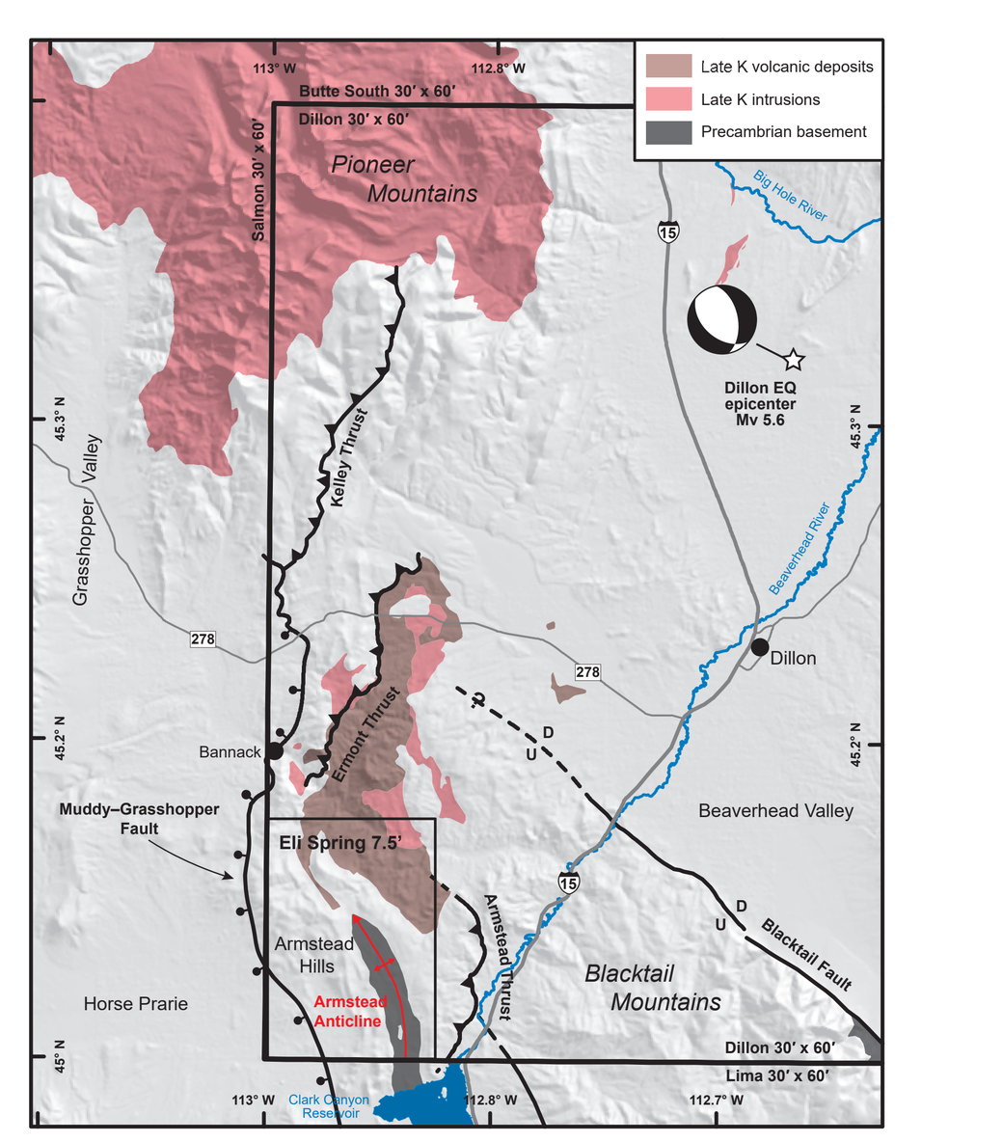

Figure 1. Derivative geologic map of the Dillon area overlain on a shaded digital elevation model (DEM). The large box shows the boundary of the Dillon 30' x 60' quadrangle, and the small box shows the location of the Eli Spring 7.5' quadrangle.

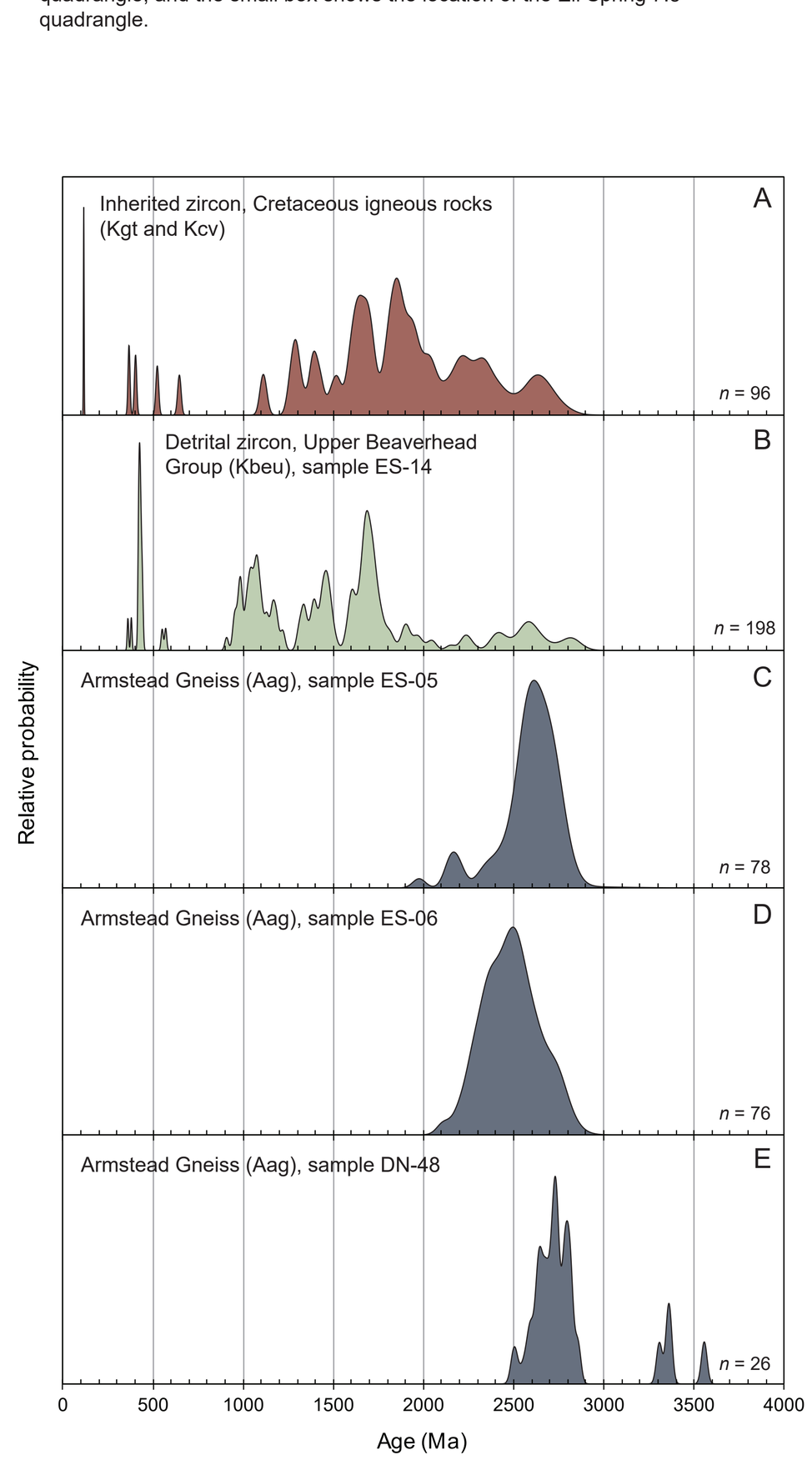

Figure 2. Probability density plots of the ^{207}Pb corrected $^{206}Pb/^{238}U$ (<1,400 Ma) and $^{207}Pb/^{206}Pb$ (>1,400 Ma) zircon ages from metamorphic, volcanic, and sedimentary rock samples. (A) Inherited zircon, Cretaceous igneous rocks (samples ES-01, ES-03, ES-08, ES-12, and DN-08). (B) Detrital zircon ages for a sandstone in the Upper Beaverhead Group (Kbeu). (C–E) Zircon ages from the Armstead Gneiss (Aag).

PHYSIOGRAPHIC AND TECTONIC SETTING

The Eli Spring 7.5' quadrangle is located in Beaverhead County, approximately 28 km (17.4 mi) southwest of Dillon, MT, and 1.5 km (0.9 mi) north of Clark Canyon Reservoir (fig. 1). The quadrangle covers part of the Armstead Hills in the northern Tendoy Mountains, a region characterized by moderate relief and elevations ranging from 1,677–2,306 m (5,500–7,567 ft). Tilted Paleozoic strata generally form resistant, north-northwest trending ridges that rise above the recessive Archean basement and Cretaceous volcanogenic and sedimentary units. Bedrock exposure is excellent with minimal vegetative cover.

The map is located near the leading edge of the Cordilleran fold-thrust belt in an area an area of presumed overlap between thin- and thick-skinned contractional structures (e.g., Johnson, 1986; Johnson and Sears, 1988). Local crustal shortening in the Armstead Hills was synorogenic with Late Cretaceous magmatism and associated sedimentation (e.g., Kalakay, 2001) that accompanied the eastward migration of the Cordilleran magmatic front (e.g., Decelles, 2004). Extensional faults overprint the older contractional structures in the Armstead Hills and appear to have been contemporaneous with local Cenozoic magmatism recorded by the local Dillon Volcanic Group (e.g., Fritz and others, 2007). Archean basement rock exposed in the quadrangle is near the junction of several postulated basement terranes including the Wyoming Province, Archean Medicine Hat block, Paleoproterozoic Great Falls Tectonic Zone, and the Mesoproterozoic Belt Basin (e.g., Foster and others, 2012).

GEOLOGIC SUMMARY

The oldest rock in the map is a heterogeneous assemblage of Archean gneiss and high-grade metasedimentary sequences collectively mapped as the Armstead Gneiss (Aag). This metamorphic assemblage provides a record of temporally distinct tectonothermal events circa ~2.7 Ga, ~2.5–2.4 Ga, and ~1.8 Ga. A sequence of Paleozoic–Triassic carbonates and interbedded siliciclastic rocks (Cf–JTRed) over ~1.5 km thick (4,920 ft) rests on a nonconformable contact cutting the Archean metamorphic rocks. These sedimentary sequences record several marine incursions across the western edge of the North American Craton. Overlying Late Cretaceous sedimentary strata (Kk) mark the transition from marine to continental sedimentation during the late Mesozoic, presumably in the foreland of the Cordilleran fold-thrust belt (e.g., Decelles, 2004). Younger synorogenic sedimentary deposits (Kbel and Kbeu) and intercalated volcanic units (Kgt, Kcv, and Kms) record the onset of local thrust-belt deformation and contemporaneous magmatism in the Eli Spring quadrangle.

Cordilleran thrust-belt structures in the map comprise northwest-striking contractional faults and east-verging folds in the Cambrian through Late Cretaceous sedimentary and igneous units, and involve crystalline basement rocks (Aag) exposed in the core of the Armstead Anticline. The shortening structures formed in the hanging wall of the Armstead Thrust Fault to which they are structurally linked (fig. 1; Coryell, 1983; Johnson, 1986; Mosolf, in prep[a].). New geothermochronology constraints reported herein indicate the thrust-belt structures were active circa ~100–66 Ma.

Extensional structures overprint and reactivate the older thrust-belt structures. Poorly lithified Tertiary sedimentary deposits (Tml) exposed in the southwestern part of the map area were coeval with extensional faulting during Eocene–Oligocene time, accumulating in a half-graben formed by the Muddy–Grasshopper Fault (VanDenburg and others, 1998). Thin intervals of ostensibly younger gravel deposits (Tsc) blanket the central part of the map area.

Extensive Quaternary deposits of alluvium, colluvium, and talus cover the bedrock locally. Landslide deposits occur throughout the map area, most of which are formed in Cretaceous volcanic and Tertiary sedimentary deposits. The area was not glaciated.

PREVIOUS MAPPING

Parts of the Eli Spring 7.5' quadrangle are included in a small-scale map by Ruppel and others (1993, scale 1:250,000) and larger-scale maps by Lowell (1965, scale 1:31,680), Coryell (1983, scale 1:12,000), Johnson (1986; scale 1:24,000), and Kalakay (2001). Mapping of the Late Cretaceous volcanic stratigraphy is based on work by Ivy (1988). The Tertiary sedimentary stratigraphy is correlated to units mapped in the adjacent Salmon 30' x 60' quadrangle (Lonn and others, 2019). Unit descriptions and thicknesses for the Paleozoic and Mesozoic stratigraphy are adapted from Coryell (1983) and Tysdal (1988). Unit descriptions of the Precambrian units are modified from Young (1982).

METHODS

Field mapping

Geologic mapping in the Eli Spring 7.5' quadrangle was conducted over one field season in 2018 (3.5 mo) as part of the U.S. Geological Survey STATEMAP program. The quadrangle was chosen to investigate the style and tempo of thrust-belt deformation and coeval magmatism, utilizing a combination of field and analytical techniques. A 1:24,000-scale topographic base and high-resolution satellite imagery were used for field mapping. Structure and observational data were located using a handheld GPS device; structure data were measured with a traditional hand transit or electronic mobile device. Field sheets were scanned and georegistered in ArcGIS. The geologic data were subsequently digitized to a geodatabase template provided by the National Cooperative Geologic Mapping Program.

Major and trace element chemistry, U-Pb geochronology, and (U-Th)/He thermochronology

Rock samples collected for whole-rock geochemistry, U-Pb geochronology, and (U-Th)/He thermochronology were crushed at the MBMG mineral separation laboratory. For geochemical analyses, a ~100–200 g split of the crushed material was prepped and analyzed by X-ray fluorescence (XRF) and inductively coupled plasma mass spectrometry (ICP-MS) at the Peter Hooper GeoAnalytical Lab, Washington State University, Pullman. Apatite and zircon were isolated from select specimens using standard pulverizing, density, and magnetic separation techniques at the MBMG mineral separation laboratory. U-Pb dating of zircon separates by Laser Ablation ICP-MS was done at the University of California, Santa Barbara. Zircon and apatite separates selected for thermochronology investigations were further prepped at the Arizona Radiogenic Helium Dating Laboratory and analyzed by Solution Sector ICP-MS.

Whole-rock chemical data are provided in table 1 and appendix A. All Laser Ablation ICP-MS geochronology data are provided in appendix B. The weighted mean of the ^{207}Pb corrected $^{206}Pb/^{238}U$ zircon ages from igneous samples are reported in table 2; $^{206}Pb/^{238}U$ (<1,400 Ma) or $^{207}Pb/^{206}Pb$ (>1,400 Ma) age distributions for sedimentary and metamorphic rocks are shown in figure 2. (U-Th)/He thermochronology results are summarized in table 3 and the associated analytical data are provided in appendices C and D. HeFTy modeling software (Ketcham, 2005, 2017) was used to create an inverse thermal model of the low-temperature thermochronological data (fig. 3). A description of all laboratory and modeling methods accompanies each respective appendix. All data appendices are available for download from the MBMG website.

DESCRIPTION OF THE MAP UNITS

The map shows rock units exposed at the surface or underlain by a thin surficial cover of soil and colluvium. Surficial sedimentary and mass movement deposits are shown where they are thick and extensive enough to be mapped at 1:24,000-scale. Igneous rocks and metamorphic rocks are classified using the International Union of Geological Sciences nomenclature (Le Bas and Streckeisen, 1991; Schmid and others, 2007). Minerals in igneous and metamorphic rock units are listed in order of decreasing abundance. Grain size classification of unconsolidated and consolidated sediment is based on the Wentworth scale (Lane, 1947). Multiple lithologies within a rock unit are listed in order of decreasing abundance.

ANTHROPOGENIC DEPOSITS

md Mining dumps (Quarternary: Holocene)—Artificial fill composed of excavated, transported, processed, and emplaced rock and gravel. Consists mainly of dredged placer workings and dumps from lode mines.

ALLUVIAL AND COLLUVIAL DEPOSITS

Grasshopper Creek, in northeastern corner of the quadrangle, is the only perennial stream in the map area and flows eastward towards its confluence with the Beaverhead River. Alluvial deposits along Grasshopper Creek have been extensively mined for placer gold in the Armstead Hills region. Widespread colluvium and talus piles cover the bedrock geology locally.

Qal **Alluvium (Quaternary: Holocene)**—Poorly sorted gravel, sand, silt, and clay along streams and their tributaries. Clasts are generally cobble size and smaller, and are subrounded to rounded. Thickness generally less than 6 m (20 ft).

Qac **Alluvium and colluvium (Quaternary: Holocene)**—Gravel, sand, and silt deposited by sheetwash alluvium and incorporated with locally derived colluvium. Commonly deposited in ephemeral stream drainages. Thickness generally less than 6 m (20 ft).

Qta **Talus (Holocene and Pleistocene)**—Unconsolidated, locally derived, apron-like deposits with angular clasts on and below steep slopes. Includes some rock-slide deposits. Variable thickness, generally less than 10 m (33 ft).

MASS WASTING DEPOSITS

Qls **Landslide deposit (Quaternary: Holocene)**—Unstratified, poorly sorted rock fragments deposited by slumps, slides, and debris flows. Typically characterized by hummocky topography and subdued landslide scarps. Most common in Cretaceous volcanic and Tertiary sedimentary deposits. Variable thickness, generally less than 30 m (100 ft).

TERTIARY SEDIMENTARY DEPOSITS

The oldest Tertiary sedimentary deposits (Tml) occur in the southwestern part of the map and are equivalent to the Eocene–Oligocene Medicine Lodge beds in the adjacent Salmon 30' x 60' quadrangle based on extent and lithological similarities (Lonn and others, 2019). These sedimentary accumulations are composed of poorly consolidated gravels interpreted to be proximal fluvial and debris flow deposits formed in alluvial fans. The Medicine Lodge beds likely accumulated in an extensional half-graben (proto-Medicine Lodge basin) that was structurally controlled by the Muddy–Grasshopper Fault (VanDenburg and others, 1998). Relatively thin and seemingly younger intervals of unconsolidated gravel (Tsc) rest on an unconformity truncating the Cretaceous and older map units in the central part of the quadrangle; these deposits are tentatively correlated to the Sixmile Creek Formation (Sears, 2007).

Tsc **Sixmile Creek Formation, undivided (late to middle Miocene)**—Thin, unconsolidated deposits of subrounded to rounded pebbles and cobbles. Clasts include quartzite derived from the Mesoproterozoic Belt Supergroup, Paleozoic limestone, Paleozoic quartzite, and volcanic and intrusive rock fragments. Clasts are likely recycled from the Beaverhead Group on the basis of rounding and clast composition. Poorly exposed with no discernable bedding or sedimentary structures. Thickness as much as 120 m (400 ft).

Tml **Medicine Lodge beds (Eocene–Oligocene?)**—Poorly consolidated gravel deposits consisting of subangular, pebble to cobble clasts of Mississippian limestone and quartzite. Poorly sorted with no discernable sedimentary structures. Thickness unknown.

EOCENE VOLCANIC ROCKS

A small outcrop of basalt unconformably resting on the northeastern limb of the Armstead Anticline was the only Tertiary volcanic unit identified in the map. Correlative Eocene–Oligocene basalt flows (Dillon Volcanic Group) in the adjacent Dalys 7.5' quadrangle exhibit high-K calc-alkaline signatures and are enriched in trace elements indicative of an active plate margin modified by subduction processes (Mosolf, 2016).

Tba **Basalt lavas (Tertiary: Eocene–Oligocene)**—Dark gray to black basaltic lava flows that are slightly porphyritic containing <10 percent phenocrysts of olivine, clino-, and orthopyroxene with occasional plagioclase. In thin section, the groundmass has a trachytic texture consisting of aligned microlites of plagioclase, with some olivine and pyroxene. Thickness less than 30 m (100 ft).

LATE CRETACEOUS IGNEOUS ROCKS

The oldest igneous rocks in the map are Late Cretaceous lavas, volcanic breccias, tuff deposits, and subvolcanic intrusions, all of which have intermediate to evolved compositions (fig. 4; table 1). These units generally exhibit high-K, calc-alkaline compositions and are enriched in incompatible elements indicative of subduction zone magmatism. The assimilation of country rock by parental melts is supported by significant zircon inheritance (fig. 2A), as well as the entrainment of mid- to lower-crustal xenoliths in hypabyssal intrusions and lava flows (e.g., Mosolf, in prep[b]). The extrusive volcanic units are intercalated with sedimentary strata of the Beaverhead Group and together are deformed by contractional structures.

Kms **McDowell Springs granodiorite (Late Cretaceous)**—Gray green to brown weathering granodiorite porphyry (63.0–62.6 wt. percent SiO_2; table 1) containing phenocrysts of plagioclase, pyroxene, biotite, hornblende, and rare quartz in a groundmass of plagioclase and altered mafic microlites with abundant magnetite. Exhibits flow banding and columnar jointing locally, and commonly forms sheet-like bodies up to 300 m thick (985 ft). Weathers to prominent buttes and hoodoos locally. Two samples collected in the adjacent Bannack 7.5' quadrangle yielded U-Pb zircon ages of 71.9 ± 0.7 and 71.8 ± 0.5 Ma (Mosolf, in prep[b]).

Kcv **Cold Spring Creek volcanic group (Late Cretaceous)**—Complex, intertonguing sequence of porphyritic lava flows, volcanic breccia, and ash-flow tuff. Porphyritic lavas (68.1–61.7 wt. percent SiO_2; table 1) are generally dark colored and contain crowded phenocrysts of plagioclase, orthopyroxene, clinopyroxene, hornblende, biotite, and quartz in a plagioclase-phyric groundmass with abundant Fe-Ti oxides. Intercalated volcanic breccias commonly occur as massive, greenish gray intervals 3–5 m thick (10–16 ft) composed of poorly sorted, subrounded to subangular clasts of andesite–dacite porphyry. Discontinuous tuff interbeds 2–10 m thick (6–33 ft) contain broken phenocrysts of plagioclase, hornblende, rare quartz, and accidental volcanic clasts in a eutaxitic groundmass of devitrified and flattened glass shards. Tuff intervals commonly contain varying amounts of pumice fragments and accidental clasts of porphyry lava. Four samples yielded U-Pb zircon ages spanning 72.6 ± 0.5 to 71.8 ± 0.6 Ma (table 2), and three samples collected in the adjacent Bannack 7.5' quadrangle yielded U-Pb ages ranging from 73.1 ± 0.8 to 71.7 ± 0.6 Ma (Mosolf, in prep[b]). Ivy (1988) reported $^{40}Ar/^{39}Ar$ hornblende ages spanning ~80–76 Ma for this unit. Thickness as much as 490 m (1,600 ft).

Kgt **Grasshopper Creek tuff (Late Cretaceous)**—White, light gray, yellowish gray, and pale red deposits of thin-bedded, vitric tuff and massively bedded, crystal-lithic rhyolite tuff. Contains varying proportions of sanidine, quartz, and plagioclase crystals, and accidental fragments of volcanic and sedimentary rock in a matrix of glass shards that are mostly zeolitized and silicified. Commonly exhibits compaction foliation formed by the collapse of pumice fragments; strongly welded intervals occur locally. A sample collected in the Eli Spring 7.5' quadrangle yielded a U-Pb zircon age of 74.7 ± 1.2 Ma (table 2), and a sample collected in the adjacent Bannack quadrangle yielded a U-Pb age of 73.3 ± 0.6 Ma (Mosolf, in prep[b]). Kalakay (2001) reported a SHRIMP U-Pb zircon age of 75.1 ± 1.1 Ma for this unit. Thickness as much as 300 m (1,000 ft).

MESOZOIC SEDIMENTARY ROCKS

Triassic through Late Cretaceous sedimentary strata record sedimentation in shallow marine and marginal-marine environments (JTRed) followed by extensive continental sedimentation (Kk, Kbel, and Kbeu) linked to the growth and eastward propagation of the Cordilleran fold-thrust belt. Clast compositions and detrital zircon of the Beaverhead Group (Kbel and Kbeu) indicate these synorogenic deposits were derived from the erosion of Proterozoic–Paleozoic formations exhumed in the hinterland of the Cordilleran fold-thrust belt (fig. 2B) with max depositional ages spanning approximately 77.9–65.9 Ma (Laskowski and others, 2013; Garber and others, 2020). The stratigraphic subdivisions of the Beaverhead Group are inconsistent in the literature, due in part to the correlation of lithologically complex and laterally discontinuous units. Informal subdivisions used in this map follow the nomenclature defined by Lowell (1965) and Johnson (1986).

Kbeu **Beaverhead Group, upper (Late Cretaceous—Paleocene?)**—Poorly lithified, clast-supported conglomerate beds composed of well-rounded and imbricated pebbles and cobbles. Approximately 50–80 percent of conglomerate clasts are red to maroon weathering quartzite derived from the Belt Supergroup and the remainder are Paleozoic limestone, quartzite, chert, and rare dacite–andesite clasts that are deeply weathered. Conglomerate beds are 10–100 cm thick and have tabular and lenticular geometries. Sample ES-14 yielded a broad distribution of detrital zircon ages with prominent peaks at ~360–600 Ma, ~900–2,100 Ma, and ~2,200–2,900 Ma (fig. 2B). While no Cretaceous ages were recovered from sample ES-14, detrital zircon max depositional ages of 65.9 ± 1.3 and 71.6 ± 3.4 Ma were reported for the upper Beaverhead Group in the adjacent Dalys and Bannack 7.5' quadrangles, respectively (Laskowski and others, 2013; Garber and others, 2020). Thickness as much as 400 m (1,300 ft).

Kbel **Beaverhead Group, lower (Late Cretaceous)**—Reddish brown to gray weathering, clast-supported conglomerate consisting of 1–10 m thick (3–33 ft) beds of subangular to rounded pebbles and cobbles. Clasts are mostly derived from Mississippian limestone with some quartzite clasts (<10 percent). Minor interbeds of sandstone are composed primarily of carbonate-cemented, medium- to coarse-grained quartz and chert sand. Underlain by a discontinuous andesite tuff in the adjacent Bannack 7.5' quadrangle that yielded a U-Pb zircon age of 79.3 ± 1.3 Ma (Murphy, 2000; Kalakay, 2001). Laskowski and others (2013) reported a detrital zircon max depositional age of 77.9 ± 1.3 Ma for a sample collected in the Bannack quadrangle. Thickness as much as 900 m (2,950 ft).

Kk **Kootenai Formation, undivided (Late Cretaceous)**—Three informal members (lower, middle, and upper) of the Kootenai Formation have been previously described in the nearby Blacktail Mountains (Tysdal, 1988), but only the middle and lower members are exposed in the map. The middle member is 120 m (400 ft) thick and is composed of reddish orange to maroon mudstone, siltstone, and minor sandstone, all of which are poorly exposed and form red weathering slopes. The lower member is 30–60 m thick (100–200 ft) and consists of white, medium-bedded, poorly cemented quartz sandstone and pebble conglomerate containing white quartz and black chert clasts; these intervals commonly form resistant ridges. The Kootenai Formation is eroded or covered by Quaternary deposits locally; minimum thickness is estimated to be approximately 50 m (165 ft) where overlain by Kbel, and 150 m (490 ft) in the Hans Peterson Flats in the southwestern corner of the map.

JTRed **Swift and Dinwoody Formations, undivided (Jurassic–Triassic)**

Swift Formation (Jurassic)—Green gray to pale green interbeds of marl, conglomerate, and shale. Fine-grained, laminated marl beds are 2–20 cm thick (1–8 in) and contain glauconite and occasional chert fragments. Conglomerate intervals are composed of poorly sorted pebble-sized clasts of quartz, black chert, green shale, and fossiliferous limestone in a calcareous to argillaceous matrix. Planar interbeds of red brown, argillaceous shale are 2–5 cm thick (1–2 in). Thickness as much as 13 m (42 ft).

Dinwoody Formation (Triassic)—Interbedded shale, limestone, and calcareous sandstone characterized by platy, thinly laminated beds that weather a distinctive chocolate brown to light gray. The upper part of the formation is composed of interbedded shale and calcareous sandstone beds and massive, gray weathering carbonate intervals. The lower part of the formation consists mostly of olive fissile shale interbedded with dark brown, silty limestone beds. Thickness as much as 200 m (655 ft).

PALEOZOIC SEDIMENTARY ROCKS

Mississippian through Permian strata exhibit marine and marginal-marine facies that record multiple marine incursions into southwest Montana. Previous work inconsistently refers to the Mississippian units as either the Snowcrest Range Group or the Amsden Formation and Big Snowy Group. The Snowcrest Range Group is adopted here (after Wardlaw and Pecora, 1985), which includes the Conover Ranch, Lombard, and Kibbey Formations.

Pp **Phosphoria Formation (Late Permian)**—From top to bottom, the formation includes interbedded yellowish brown, fine- to medium-grained glauconitic quartz sandstone; dark gray to black finely layered phosphatic mudstone; light gray dolomite that contains nodular chert and chert stringers; pale brown phosphatic mudstone; and pale brown, thin-bedded mudstone and interbedded sandstone. Bed thickness ranges from 10–35 cm (4–14 in) in dolomites, and 5–35 cm (2–14 in) in cherts and sandstones. Chert-rich intervals form resistant outcrops, otherwise recessive and poorly exposed. Thickness is approximately 100 m (350 ft).

IPq **Quadrant Formation (Pennsylvanian)**—Light gray to light yellowish brown, fine- to medium-grained, medium- to thick-bedded, vitreous, quartz sandstone. Trough crossbedding is common. Forms resistant ridges and cliffs that are typically covered with conifers. As thick as 300 m (985 ft).

IPMsr **Snowcrest Range Group, undivided (Late Mississippian to Pennsylvanian)**—Interbedded mudstone, siltstone, sandstone, and carbonate composing the Conover Ranch, Lombard, and Kibbey Formations; mapped as one unit. The thickness of individual formations was undetermined; total group thickness estimated to be 290–300 m (950–985 ft).

Conover Ranch Formation—Thin-bedded, red calcareous mudstone with minor interbeds of limestone, calcareous sandstone, and siltstone. Contains a medium-bedded, limestone pebble conglomerate interval at the base. Poorly exposed and commonly forms a slope beneath the Quadrant Formation.

Lombard Formation—Mapping by Tysdal (1988) and a restoration of a deformed section by Pecora (1981) show the formation to consist of three informal members in the nearby Blacktail Mountains. The upper member is pale brown to gray, thin- to thick-bedded crinoidal limestone and dark gray limey shale. The middle member is composed of pale brown to light gray, thin- to thick-bedded limestone; interbeds of siltstone and claystone; and a discontinuous bituminous coal seam. The lower member is olive gray to pale red purple, thin- to thick-bedded limestone with ostracod-rich horizons. Contains detachment folds locally.

Kibbey Formation—Pale yellow, yellowish orange, and reddish brown thin-bedded argillaceous fine-grained quartz sandstone. Lower sandstone beds contain black chert grains. Poorly exposed and generally forms slopes beneath the Lombard Formation.

Mmc **Mission Canyon Formation (Mississippian)**—Light gray, medium- to thick-bedded and locally massive limestone, oolitic limestone, and dolomitic limestone. Contains zones of evaporate-solution breccia and intervals of bioclastic debris consisting of crinoids, bryozoans, and brachiopods. Chert stringers are common and often coincide with bedding planes. Forms prominent outcrops and cliffs. Thickness estimated to be 400 m (1,310 ft).

Ml **Lodgepole Formation (Mississippian)**—Light to dark gray, thin- to medium-bedded limestone, mudstone, and red calcareous siltstone. Beds are planar to undulose and rhythmically bedded. The formation is abundantly fossiliferous, including bioclasts of crinoids, bryozoans, and brachiopods. Forms outcrops on steep slopes. Thickness estimated to be 370 m (1,210 ft).

MDtj **Three Forks and Jefferson Formations, undivided (Mississippian and Devonian)**—Interbedded shale, sandstone, limestone, and dolomite. Mapped as a single unit. Total thickness estimated to be 170 m (560 ft).

Three Forks Formation (Mississippian and Devonian)—Brown, argillaceous, fossiliferous limestone interlayered with black to dark gray, carbonaceous shale, grayish green slaty shale, and light tan, silty sandstone. Recessive and mapped on the basis of float. Thickness approximately 30 m (100 ft).

Jefferson Formation (Devonian)—Dark gray to brown, coarsely crystalline, medium- to thick-bedded dolomite with thin interbeds of yellowish brown calcareous siltstone. Dolomite beds emit a strong petroliferous odor. Algal laminations occur near the base of the formation and flat pebble conglomerate occurs near the top. Contains some soft sediment deformation. White and orange lichen grow on rock outcroppings. Thickness is approximately 140 m (460 ft).

Ch **Hasmark Formation (Late Cambrian)**—Light gray to white, thin- to thick-bedded, crystalline dolomite with minor shale and limestone intervals. Weathers to a conspicuous light gray to pale brown color with a gritty, laminated surface. Forms ridges and cliffs. Thickness is approximately 70–80 m (230–260 ft).

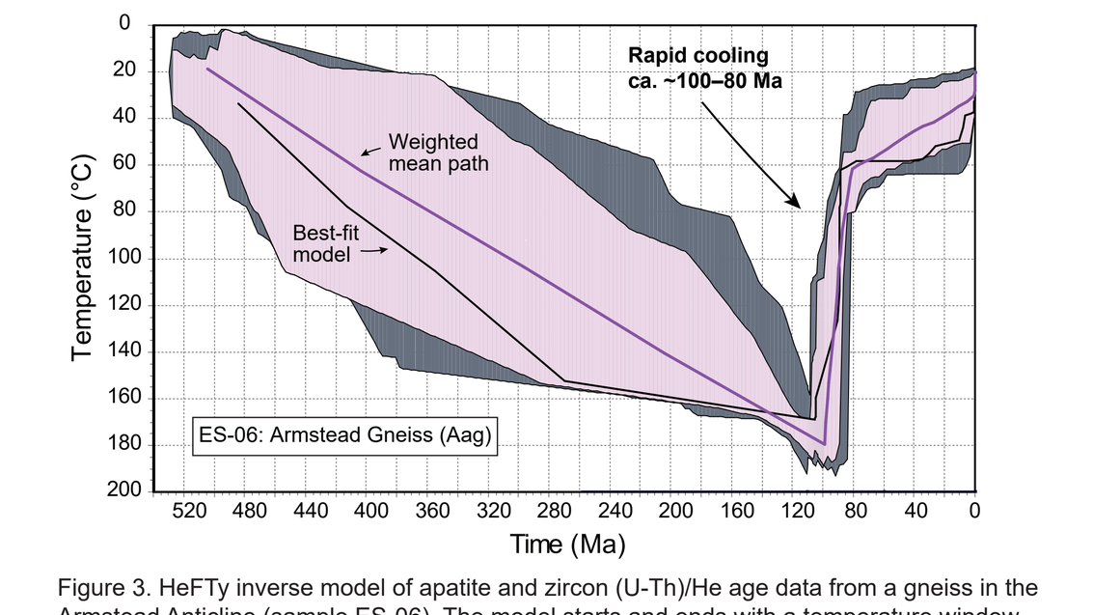

Figure 3. HeFTy inverse model of apatite and zircon (U-Th)/He age data from a gneiss in the Armstead Anticline (sample ES-06). The model starts and ends with a temperature window between 0°C and 40°C ca. 530–480 Ma and 0 Ma. Additional time-temperature model constraints were imposed at 120–200°C ca. 110–60 Ma, and 30–80°C ca. 100–50 Ma. The results are colored by Goodness of Fit (GOF) statistical modeling (model age vs. measured age). The gray envelope shows acceptable-fit paths (GOF > 0.05 to 0.5); the pink envelope shows good-fit paths (GOF > 0.5); the purple line is the weighted mean path, and the black line is the best-fit model path. See Appendices C and D for supporting information.

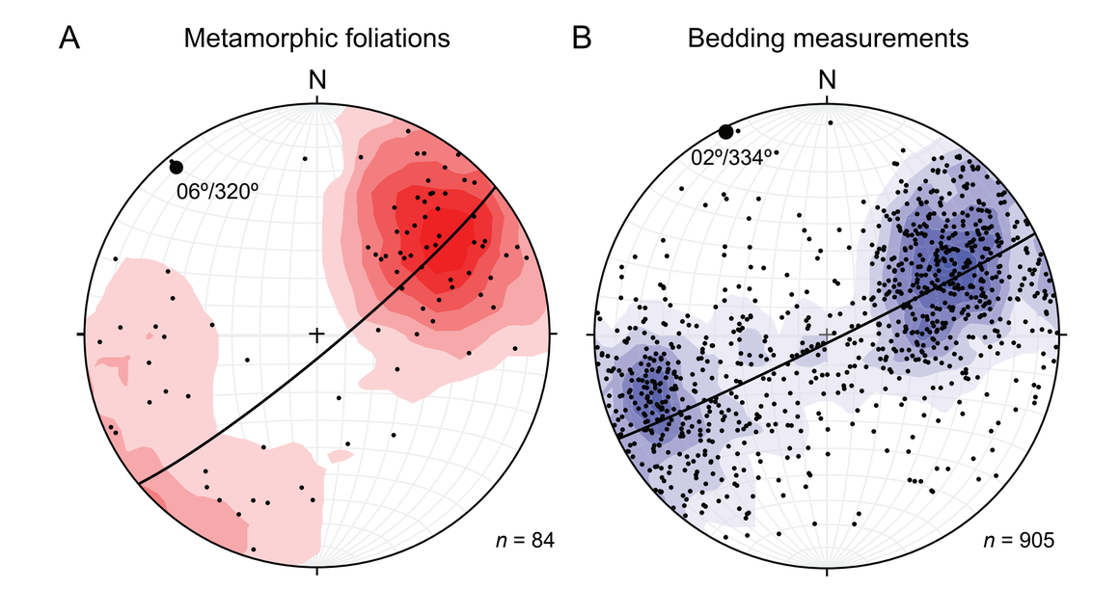

Figure 5. Lower-hemisphere projection of poles to bedding and foliation measurements. The data are plotted on equal-area stereonets and fit with Kamb contours. The great circles represent the cylindrical best fit with the corresponding fold hinges marked by black dots labeled by plunge and trend. (A) Metamorphic foliations in the Armstead Gneiss (Aag). The distribution shows most foliations dip southwest with some folding about an axis plunging gently to the northwest (06°/320°). (B) Bedding measurements acquired in the Paleozoic through Late Cretaceous units. The distribution reflects folding about an axis plunging gently northeast (02°/034°).

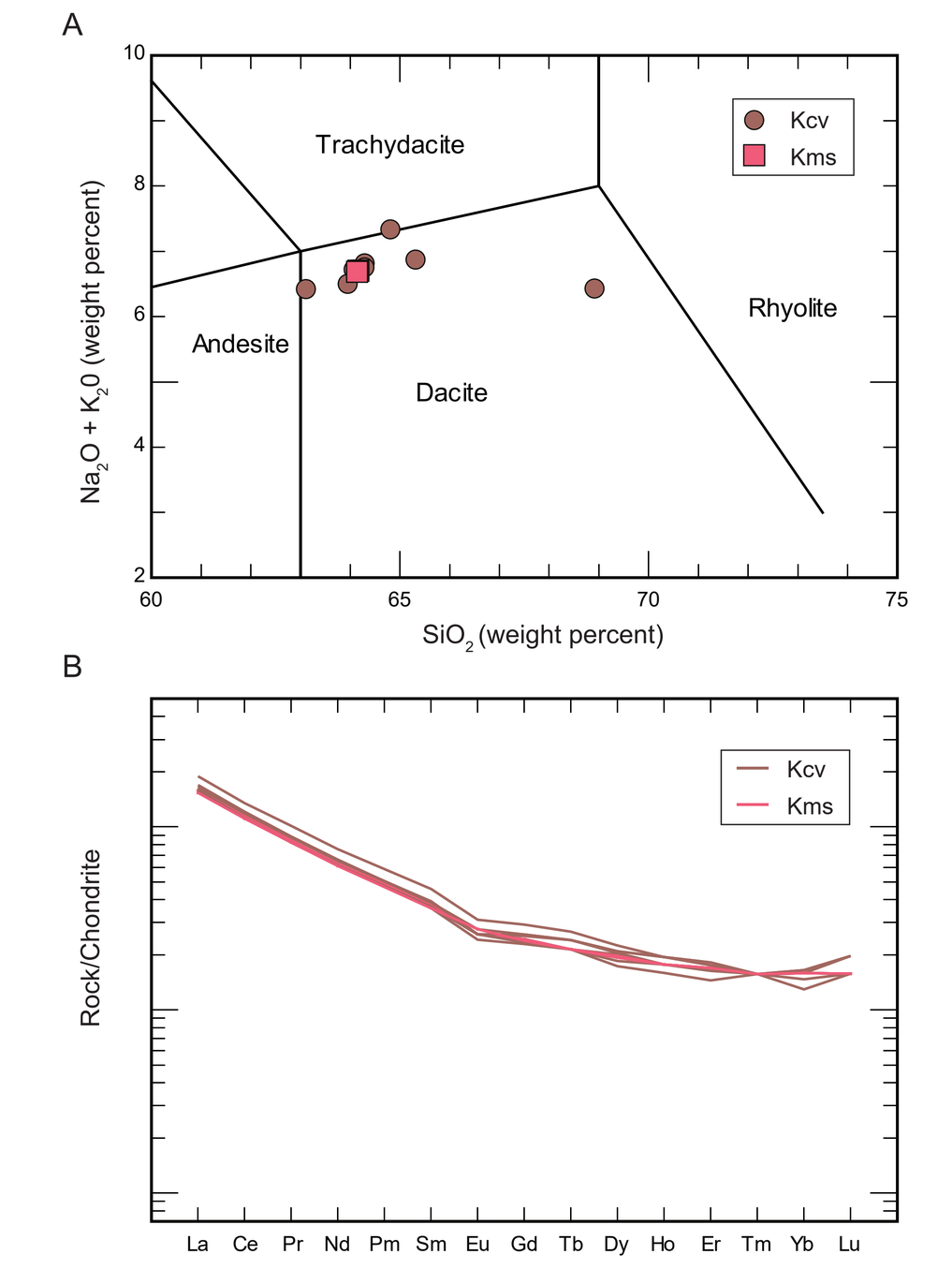

Figure 4. Whole-rock geochemical data from Cretaceous volcanic rocks. (A) Total alkali silica classification diagram (after Le Bas and others, 1986). Plotted values are normalized to 100 percent. (B) Chondrite-normalized rare earth element plot (after Sun and McDonough, 1989).

Table 1. Major oxide and trace element geochemistry.

Sample ID	ES-02	ES-03	ES-05	ES-06	ES-07	ES-08	ES-09*	ES-10	ES-11	ES-12	ES-13	DN-08
Map unit	Kcv	Kcv	Aag	Aag	Kcv	Kcv	Kcv	Kms	Kcv	Kcv	Kms	Kcv
Lithology	Dacite lava	Dacite lava	Gneiss	Gneiss	Dacite lava	Dacite lava	Dacite lava	Dacite intrusion	Dacite lava	Dacite lava	Dacite intrusion	Dacite lava
Latitude (°N)	45.1008	45.1021	45.0170	45.0081	45.0746	45.0768	45.1109	45.1118	45.0902	45.0971	45.1224	45.1023
Longitude(°W)	112.9344	112.9730	112.8939	112.8908	112.8944	112.8842	112.9265	112.9045	112.9043	112.8955	112.9025	112.8863
Major elements (wt%)												
SiO_2	61.70	63.08	75.81	70.96	62.61	62.99	68.14	62.99	62.34	63.29	62.57	64.13
TiO_2	0.70	0.60	0.41	0.55	0.54	0.54	0.55	0.56	0.54	0.56	0.55	0.57
Al_2O_3	16.41	15.50	9.69	13.63	16.61	16.57	14.97	16.55	16.65	16.56	16.61	16.39
FeO*	5.81	5.74	3.97	3.07	5.05	4.93	4.21	5.16	5.03	5.11	5.12	5.25
MnO	0.09	0.12	0.03	0.05	0.11	0.10	0.05	0.10	0.11	0.11	0.09	0.06
MgO	1.91	1.18	2.38	0.48	1.59	1.51	0.39	1.56	1.75	1.45	1.50	0.62
CaO	4.69	3.81	0.19	1.99	4.47	4.48	4.05	4.51	4.55	4.55	4.43	4.24
Na_2O	3.42	3.33	1.45	3.11	3.98	3.91	3.47	3.91	3.69	3.88	3.89	3.82
K_2O	2.84	3.79	3.91	5.19	2.57	2.75	2.87	2.67	2.63	2.75	2.63	2.91
P_2O_5	0.17	0.16	0.04	0.13	0.16	0.16	0.15	0.16	0.16	0.16	0.17	0.17
Sum	97.73	97.32	97.88	99.18	97.69	97.97	98.85	98.17	97.45	98.41	97.56	98.16
LOI	1.79	2.19	1.61	0.30	1.62	1.31	0.69	1.36	1.93	0.93	1.94	1.25
Trace elements (ppm)												
Ni+	4.5	3.3	29.9	4.3	3.0	2.7	9.2	3.8	4.7	4.1	3.0	5.8
Cr+	14.3	7.8	7.0	6.9	7.4	7.2	10.5	6.7	6.3	7.3	6.2	4.2
V+	101.0	71.4	8.2	25.1	75.5	75.5	62.3	77.4	70.3	79.3	76.3	79.6
Ga+	19.5	17.9	15.9	16.5	18.7	18.1	16.9	18.1	18.4	17.7	18.7	18.7
Cu+	10.7	12.5	60.1	1.4	8.5	7.4	10.0	8.7	7.4	7.7	8.6	6.9
Zn+	81.4	67.5	15.1	48.6	72.6	73.1	40.4	73.5	74.9	74.6	73.9	80.2
La	44.7	39.5	80.0	64.9	37.3	37.2	38.3	37.4	38.8	40.1	36.3	37.5
Ce	82.5	72.8	151.2	131.8	69.1	68.9	71.3	69.7	72.9	73.9	67.8	68.1
Pr	9.6	8.3	17.2	14.2	7.8	7.9	8.0	8.0	8.3	8.4	7.8	7.8
Nd	35.2	30.6	62.3	49.1	28.8	28.8	28.7	29.3	30.4	30.9	28.5	28.7
Sm	7.0	5.9	11.9	9.6	5.6	5.6	5.5	5.8	6.0	5.9	5.5	5.6
Eu	1.8	1.5	2.7	2.2	1.5	1.5	1.4	1.5	1.5	1.6	1.6	1.5
Gd	6.0	5.2	9.7	8.6	5.0	5.0	4.7	5.0	5.3	5.3	4.9	4.8
Tb	1.0	0.9	1.5	1.6	0.8	0.8	0.8	0.8	0.9	0.9	0.8	0.8
Dy	5.7	5.2	9.0	10.1	5.0	5.1	4.4	5.0	5.3	5.3	4.9	4.7
Ho	1.1	1.0	1.8	2.2	1.0	1.0	0.9	1.0	1.1	1.1	1.0	1.0
Er	3.0	2.8	5.2	6.3	2.8	2.8	2.4	2.8	3.0	2.9	2.8	2.7
Tm	0.4	0.4	0.8	1.0	0.4	0.4	0.4	0.4	0.4	0.4	0.4	0.4
Yb	2.7	2.7	5.2	6.4	2.7	2.7	2.2	2.7	2.8	2.8	2.7	2.5
Lu	0.4	0.4	0.8	1.0	0.5	0.4	0.4	0.4	0.5	0.5	0.4	0.4
Ba	1063.6	1366.8	1534.0	1366.4	1295.6	1307.3	1294.6	1287.4	1325.3	1353.9	1294.4	1371.3
Th	9.2	8.8	30.5	24.8	8.6	8.6	8.4	8.8	8.5	9.0	8.3	8.5
Nb	13.0	12.4	23.5	27.2	13.6	13.7	13.6	13.5	13.7	13.6	13.4	13.8
Y	29.1	27.2	44.7	57.6	27.0	26.9	23.7	26.9	27.8	28.2	25.8	25.1
Hf	6.5	6.0	19.5	11.3	5.8	5.8	5.6	5.5	5.6	6.0	5.6	5.9
Ta	0.9	0.8	0.9	2.1	0.9	0.9	0.9	0.9	0.9	0.9	0.9	0.9
U	2.1	1.6	2.8	1.8	2.3	2.8	2.1	2.3	2.3	2.3	1.8	1.9
Pb	19.9	17.3	18.7	20.7	20.5	21.2	22.8	20.0	21.5	20.9	20.1	18.9
Rb	80.6	96.3	62.5	213.5	78.7	75.8	82.2	75.7	103.0	76.0	74.1	80.2
Cs	0.7	0.5	0.5	1.0	1.6	1.6	1.4	1.3	2.1	1.5	1.3	1.4
Sr	415.8	463.1	31.6	108.9	553.2	554.2	519.5	520.3	567.5	562.3	517.8	551.0
Sc	11.6	11.4	5.9	4.6	9.8	9.3	9.4	8.6	9.4	9.3	9.3	8.5
Zr	253.4	237.5	750.6	419.0	227.7	227.5	231.3	214.4	223.9	237.2	221.7	234.3

Note. All major elements and trace elements denoted by + were analyzed by XRF, all other trace elements were measured by ICP-MS. FeO* indicates all Fe expressed as Fe^{2+}. LOI is loss on ignition. All samples analyzed by X-ray fluorescence (XRF) and inductively coupled plasma mass spectrometry (ICP-MS) at the Washington State University GeoAnalytical Lab. Latitudes and longitudes are in the 1984 World Geodetic Survey (WGS84) datum.
*clast from volcanic breccia.

Table 2. U-Pb zircon geochronology.

Sample	Lithology	Unit	Latitude (°N)	Longitude (°W)	# of spot analyses[a]	Age (Ma)	2σ	MSWD
DN-08	Pumice-lithic tuff	Kcv	45.1023	112.8863	16	71.8	0.6	1.0
ES-01	Rhyolitic tuff	Kgt	45.1171	112.9546	10	74.7	1.2	2.0
ES-03	Dacite lava	Kcv	45.1021	112.9730	10	72.5	0.8	1.1
ES-08	Dacite lava	Kcv	45.0768	112.8842	20	72.0	0.5	0.7
ES-12	Dacite lava	Kcv	45.0971	112.8955	19	72.6	0.5	1.0

Note. Reported ages are the weighted mean of the ^{207}Pb corrected $^{206}Pb/^{238}U$ ages obtained for each sample. MSWD is the Mean Square Weighted Deviation. Zircon separates were prepared at MBMG and analyzed by LA-ICPMS at the University of California, Santa Barbara. Latitudes and longitudes are in the 1984 World Geodetic Survey (WGS84) datum.
[a]number of spot analyses used to calculate weighted mean age.

Table 3. (U-Th)/He apatite and zircon thermochronology data.

Sample ID	Mineral	Map unit	Latitude (°N)	Longitude (°W)	Elevation (m)	Mass (µg)	Rs (µm)	eU (ppm)	U (ppm)	Th (ppm)	He (nmol/g)	Ft ^{238}U	Ft ^{235}U	Ft ^{232}Th	Ft ^{147}Sm	Corrected age (Ma)	2σ age (Ma)
Sample DN-48:																	
DN48_a1	apatite	Aag	45.0497	112.9065	[illegible]	[illegible]	[illegible]	[illegible]	[illegible]	[illegible]	[illegible]	[illegible]	[illegible]	[illegible]	[illegible]	[illegible]	[illegible]
DN48_a2	apatite	Aag	45.0497	112.9065	[illegible]	[illegible]	[illegible]	[illegible]	[illegible]	[illegible]	[illegible]	[illegible]	[illegible]	[illegible]	[illegible]	[illegible]	[illegible]
DN48_a3	apatite	Aag	45.0497	112.9065	[illegible]	[illegible]	[illegible]	[illegible]	[illegible]	[illegible]	[illegible]	[illegible]	[illegible]	[illegible]	[illegible]	[illegible]	[illegible]
DN48_a4	apatite	Aag	45.0497	112.9065	[illegible]	[illegible]	[illegible]	[illegible]	[illegible]	[illegible]	[illegible]	[illegible]	[illegible]	[illegible]	[illegible]	[illegible]	[illegible]
DN48_z1	zircon	Aag	45.0497	112.9065	[illegible]	[illegible]	[illegible]	[illegible]	[illegible]	[illegible]	[illegible]	[illegible]	[illegible]	[illegible]	[illegible]	[illegible]	[illegible]
DN48_z2	zircon	Aag	45.0497	112.9065	[illegible]	[illegible]	[illegible]	[illegible]	[illegible]	[illegible]	[illegible]	[illegible]	[illegible]	[illegible]	[illegible]	[illegible]	[illegible]
DN48_z3	zircon	Aag	45.0497	112.9065	[illegible]	[illegible]	[illegible]	[illegible]	[illegible]	[illegible]	[illegible]	[illegible]	[illegible]	[illegible]	[illegible]	[illegible]	[illegible]
Sample ES-06:																	
ES06_a1	apatite	Aag	45.0081	112.8908	[illegible]	[illegible]	[illegible]	[illegible]	[illegible]	[illegible]	[illegible]	[illegible]	[illegible]	[illegible]	[illegible]	[illegible]	[illegible]
ES06_a2	apatite	Aag	45.0081	112.8908	[illegible]	[illegible]	[illegible]	[illegible]	[illegible]	[illegible]	[illegible]	[illegible]	[illegible]	[illegible]	[illegible]	[illegible]	[illegible]
ES06_a3	apatite	Aag	45.0081	112.8908	[illegible]	[illegible]	[illegible]	[illegible]	[illegible]	[illegible]	[illegible]	[illegible]	[illegible]	[illegible]	[illegible]	[illegible]	[illegible]
ES06_a4	apatite	Aag	45.0081	112.8908	[illegible]	[illegible]	[illegible]	[illegible]	[illegible]	[illegible]	[illegible]	[illegible]	[illegible]	[illegible]	[illegible]	[illegible]	[illegible]
ES06_a5	apatite	Aag	45.0081	112.8908	[illegible]	[illegible]	[illegible]	[illegible]	[illegible]	[illegible]	[illegible]	[illegible]	[illegible]	[illegible]	[illegible]	[illegible]	[illegible]
ES06_z1	zircon	Aag	45.0081	112.8908	[illegible]	[illegible]	[illegible]	[illegible]	[illegible]	[illegible]	[illegible]	[illegible]	[illegible]	[illegible]	[illegible]	[illegible]	[illegible]
ES06_z2	zircon	Aag	45.0081	112.8908	[illegible]	[illegible]	[illegible]	[illegible]	[illegible]	[illegible]	[illegible]	[illegible]	[illegible]	[illegible]	[illegible]	[illegible]	[illegible]
ES06_z3	zircon	Aag	45.0081	112.8908	1,825	17.0	77.9	306	273	143	481	0.841	0.818	0.818	0.950	337.5	9.0
ES06_z4	zircon	Aag	45.0081	112.8908	1,825	7.3	59.3	229	201	117	413	0.795	0.765	0.765	0.935	409.4	10.9
ES06_z5	zircon	Aag	45.0081	112.8908	1,825	13.0	65.7	456	402	231	502	0.814	0.786	0.786	0.941	246.5	7.0
Sample ES-05:																	
ES05_z1	zircon	Aag	45.0170	112.8939	1,800	1.8	36.6	214	196	79	482	0.680	0.636	0.636	0.896	588.1	16.3
ES05_z2	zircon	Aag	45.0170	112.8939	1,800	2.1	43.5	281	235	198	374	0.726	0.687	0.687	0.912	333.3	8.4
ES05_z3	zircon	Aag	45.0170	112.8939	1,800	1.7	35.8	241	219	94	330	0.673	0.629	0.629	0.894	368.8	10.0
ES05_z4	zircon	Aag	45.0170	112.8939	1,800	2.0	37.5	370	324	197	570	0.686	0.643	0.643	0.899	405.9	10.7
ES05_z5	zircon	Aag	45.0170	112.8939	1,800	3.1	44.7	261	236	106	518	0.733	0.695	0.695	0.915	484.7	13.4

Note. Samples were prepared at the MBMG and analyzed at the University of Arizona, Tucson following established lab protocols. Rs is the radius of a sphere with an equivalent surface area to voume ratio as the crystal (mass-weighted radius for multi-grain aliquots). Ft is the alpha ejection correction. 2s is one-sigma error. Latitudes and longitudes are in the 1984 World Geodetic Survey (WGS84) datum.

Csh **Silver Hill Formation (Late Cambrian)**—Brown, dark red, and olive green interbeds of micaceous clay shale and thick layers of brown glauconitic quartzose siltstone. Poorly exposed, commonly forming a saddle between the Hasmark and Flathead Formations. Thickness estimated to be 70 m (225 ft).

Cf **Flathead Formation (Middle Cambrian)**—Light gray, tan, and maroon, medium- to coarse-grained, medium-bedded quartz sandstone. Commonly crossbedded with glauconite and quartz pebbles near the base of the unit. The contact with the underlying crystalline basement rocks is sharp and nonconformable. Thickness estimated to be 60 m (200 ft).

METAMORPHIC ROCKS

Archean quartzofeldspathic gneiss and high-grade metasedimentary intervals consisting of metapelite, quartzite, and calc-silicate rocks were mapped as one unit (Armstead Gneiss; Aag). These units preserve a polyphase metamorphic history, with peak metamorphism reaching granulite facies conditions (Young, 1982). U-Pb zircon data (figs. 2C–E) suggest the Armstead Gneiss protolith formed by ~2.7 Ga or older, and was subsequently metamorphosed ca. ~2.4–2.5 Ga during the Tendoy orogeny (Jones, 2008; Cramer, 2015). While no Proterozoic ages were obtained in this study, Mueller and others (2012) reported U-Pb ages of ~1.8 Ga for the Armstead Gneiss that likely reflect a tectonothermal event termed the Big Sky Orogeny (e.g., Harms and others, 2004; Cramer, 2015). The protolith of the Armstead Gneiss has been previously interpreted to represent a volcanic complex formed above an ancient subduction zone (Young, 1982; Mueller and others, 2012).

Aag **Armstead Gneiss (Archean)**—Heterogeneous assemblage of quartzofeldspathic gneiss and high-grade metasedimentary rocks. Quartzofeldspathic gneiss occurs as uniform intervals that weather to sparsely vegetated hills covered by rocky, pinkish orange soil containing abundant feldspar chips. Gneissic varieties include quartz–feldspar gneiss, quartz–feldspar–garnet gneiss, quartz–plagioclase–garnet gneiss, and quartz–orthoclase–hornblende gneiss. Thin, conformable lenses of amphibolite gneiss are commonly intercalated with the quartzofeldspathic gneiss units. Metasedimentary intervals include thinly interlayered intervals of metapelite, amphibolite, quartzofeldspathic gneiss, quartzite, and calc-silicate marble. The metasedimentary intervals are poorly exposed, commonly forming brown soil underlying low, flat, sage-covered areas. A planar mineral foliation generally parallels compositional layering, and centimeter-scale isoclinal folds are common. See Young (1982) for detailed petrographic descriptions of the Armstead Gneiss.

STRUCTURAL GEOLOGY

Precambrian deformation

Compositional layering in the Armstead Gneiss (Aag) is likely transposed layering formed during metamorphism rather than a primary stratigraphic fabric. Mineral foliations generally parallel the compositional layering except where it penetrates the noses of centimeter-scale folds. The folds are isoclinal with some being rootless and intrafolial, which are characteristic of extensive transposition. Poor exposure generally hindered the identification of possible map-scale folds in the Armstead Gneiss. Most planar mineral foliations dip steeply to the southwest (fig. 5A), however, indicating that axial surfaces of outcrop- and perhaps map-scale folds are northwest-striking and dip steeply to the southwest. Metamorphic textures and associated folds likely formed during tectonothermal events of the Tendoy or Big Sky orogenies.

Cordilleran thrust-belt deformation

A series of map-scale, mostly northwest-trending contractional faults and folds deform the Archean through Cretaceous units. At least two unnamed reverse faults are closely associated with folds in the Paleozoic–Mesozoic units near Hans Peterson Flats in the southwestern part of the map. The most notable of these faults dips approximately 20–30 degrees to the west–southwest, placing Paleozoic strata over synorogenic deposits of the Beaverhead Group. Two reverse faults, previously interpreted to be a duplex structure (Coryell and Spang, 1988), displace early Paleozoic strata and Archean basement rock in the eastern limb of the Armstead Anticline. The Armstead Thrust Fault (fig. 1) projects beneath the Eli Spring quadrangle; this fault carries Paleozoic strata over the Beaverhead Group in the adjacent Dalys 7.5' quadrangle (Lowell, 1965; Johnson, 1986; Johnson and Sears, 1988; Coryell and Spang, 1988; Mosolf, in prep[a]).

Major folds in the map include, from west to east, the Madigan Gulch Anticline, the Cedar Creek Syncline, and the Armstead Anticline (fig. 5B); all of these folds formed in the hanging wall of the Armstead Thrust Fault. The Madigan Gulch Anticline is an east-verging, asymmetrical fold with an overturned east limb and steep west limb. The Cedar Creek Syncline is an upright, cylindrical fold that becomes overturned and east-verging along the southern trace of its axial surface. The Armstead Anticline is presumed to be an arcuate, asymmetrical antiform that has been breached by erosion, exposing Archean crystalline basement rocks in its core. The structure of the Armstead Anticline is debatable and postulated to be: (1) fault-bend folding above a ramp in the Armstead Thrust Fault (Coryell and Spang, 1988); (2) a Rocky Mountain foreland structure that was later decapitated by thin-skinned thrusting (Johnson and Sears, 1988); and (3) an antiformal stack carried in the hanging wall of the frontal thrust system (Kalakay, 2001). Mapping and kinematic data presented herein support progressive deformation in the hanging wall of the Armstead Thrust, but do not discriminate between fault-bend folding or antiformal stacking. Two anomalously east–west-trending folds associated with a minor, unnamed reverse fault deform Paleozoic units in the northwest part of the map area; it's unclear if these folds reflect heterogeneous strain in a zone of overlap between the Armstead and Ermont thrust plates, or represent a second generation of folds.

Modeling of apatite and zircon (U-Th)/He data reported herein show the Armstead Gneiss was rapidly cooled from 180–60°C at ~100–80 Ma (fig. 3), which was likely driven by tectonic exhumation associated with the Armstead Thrust Fault. Radiometric dating of deformed and undeformed magmatic units indicate that upper-crustal shortening initiated no later than ~79 Ma and continued until ~72 Ma (Kalakay, 2001; Mosolf, in prep[b]; this study). To the east in the Dalys 7.5' quadrangle, detrital zircon dating of the synorogenic Upper Beaverhead Group (Kbeu) yielded a max depositional age of ~66 Ma (Garber and others, 2020). Together, these kinematic constraints bracket the timing of upper crustal shortening in the map area to ~100–66 Ma.

Cenozoic extensional deformation

The most notable extensional structure occurs in the southwestern part of the map where poorly lithified Tertiary sedimentary deposits (Tml) are in fault contact with Paleozoic–Mesozoic strata; this fault is interpreted to be the southern trace of the Muddy–Grasshopper Fault (fig. 1; VanDenburg and others, 1998; Mosolf, in prep[b]). The fault appears to dip westward, and likely inverts an older thrust fault. Fault movement appears to have been synchronous with the deposition of proximal alluvial fan deposits of the Eocene–Oligocene Medicine Lodge beds (Tml; VanDenburg and others, 1998). The other notable extensional structure in the map (named the Cameahwait Fault by Sears, 2007) displaces the southwest limb of the Armstead Anticline, and is synthetic to a normal fault cutting the Cedar Creek Syncline. The Cameahwait Fault is poorly exposed and mostly covered by Quaternary sedimentary deposits, but appears to be a high-angle fault dipping ~60–80 degrees to the southwest. The Cameahwait Fault is likely an inverted reverse fault, or a cut-off fault rooted to a subsurface thrust ramp that was reactivated upon the onset of crustal extension. Modeling of the (U-Th)/He data suggest the Armstead Gneiss underwent an additional ~25°C of cooling ca. 40–0 Ma (fig. 3) that was possibly linked to footwall exhumation of the Muddy–Grasshopper Fault or Cameahwait Fault.

ACKNOWLEDGMENTS

Connie Thomson skillfully performed mineral separations at the MBMG Mineral Separation Laboratory, and Gary Wyss assisted with SEM-CL work at Montana Technological University, Butte. Andrew Kylander-Clark graciously supported LA-ICP-MS analyses and data reduction at the University of California, Santa Barbara. Ashley and Arron Steiner directed bulk-rock geochemical analyses at the Washington State University Peter Hooper Geoanalytical Laboratory. Technical reviews of the map and analytical data by Colleen Elliott, Jeff Lonn, and Catherine McDonald significantly improved the quality and presentation of the geologic data.

REFERENCES

Coryell, J.J., 1983, Structural geology of the Henneberry Ridge area, Beaverhead County, Montana: College Station, Texas A&M University, M.S. thesis, 126 p.
Coryell, J.J., and Spang, J.H., 1988, Structural geology of the Armstead Anticline area, Beaverhead County, Montana, *in* Schmidt, C.J., and Perry, W.J., eds., Interaction of the Rocky Mountain foreland and the Cordilleran thrust belt: Geological Society of America Memoir, v. 171, p. 217–227.
Cramer, M., 2015, Proterozoic tectonometamorphic evolution of the Ruby Range, SW Montana, USA: Insights from phase equilibria modeling in situ monazite petrochronology: Missoula, University of Montana, M.S. thesis, 79 p.
DeCelles, P., 2004, Late Jurassic to Eocene evolution of the Cordilleran thrust belt and foreland basin system, western U.S.A.: American Journal of Science, v. 304, p. 105–168.
Fritz, W.J., Sears, J.W., McDowell, R.J., and Wampler, J.M., 2007, Cenozoic volcanic rocks of southwestern Montana: Northwest Geology, v. 36, p. 91–110.
Foster, D.A., Mueller, P.A., Heatherington, A., Gifford, J.N., and Kalakay, T.J., 2012, Lu/Hf systematics of magmatic zircons reveal a Proterozoic crustal boundary under the Cretaceous Pioneer batholith, Montana: Lithos, v. 142–143, p. 216–225.
Garber, K.L., Finzel, E.S., and Pearson, D.M., 2020, Provenance of synorogenic foreland basin strata in southwestern Montana requires revision of existing models for Laramide tectonism: North American Cordillera: Tectonics, v. 39, e2019TC005944, 26 p.
Harms, T.A., Brady, J.B., Burger, H.R., and Cheney, J.T., 2004, Advances in the geology of the Tobacco Root Mountains, Montana, and their implications for the history of the northern Wyoming province, *in* Brady, J.B., Burger, H.R., Cheney, J.T., and Harms, T.A., eds., Precambrian geology of the Tobacco Root Mountains, Montana: Geological Society of America Special Paper 377, p. 227–243.
Ivy, S.D., 1988, Source, evolution, and eruptive history of the Cold Spring Creek volcanics, Beaverhead County, Montana: Corvallis, Oregon State University, M.S. thesis, 132 p.
Johnson, L.M., 1986, An overlap zone between a Laramide Rocky Mountain foreland structure and Sevier-style thrust structures near Bannack, Montana: Missoula, University of Montana, M.S. thesis, 47 p., 2 sheets, scale 1:24,000.
Johnson, L.M., and Sears, J., 1988, Cordilleran thrust belt–Rocky Mountain foreland interaction near Bannack, Montana, *in* Schmidt, C.J., and Perry, W.J., eds., Interaction of the Rocky Mountain foreland and the Cordilleran thrust belt: Geological Society of America Memoir, v. 171, p. 229–236.
Jones, C., 2008, U-Pb geochronology of monazite and zircon in Precambrian metamorphic rocks from the Ruby Range, SW Montana: Deciphering geological events that shaped the NW Wyoming province: Kent, Kent State University, M.S. thesis, 119 p.
Kalakay, T.J., 2001, The role of magmatism during crustal shortening in the retroarc fold and thrust belt of southwest Montana: Laramie, University of Wyoming, Ph.D. dissertation, 204 p.
Ketcham, R.A., 2005, Forward and inverse modeling of low-temperature thermochronometry data: Reviews in Mineralogy and Geochemistry, v. 58(1), p. 275–314.
Ketcham, R.A., 2017, HeFty version 1.9.3. Program.
Lane, E.W., 1947, Report of the subcommittee on sediment terminology: Transactions of the American Geophysical Union, v. 28, no. 6, p. 936–938.
Laskowski, A.K., DeCelles, P.G., and Gehrels, G.E., 2013, Detrital zircon geochronology of Cordilleran retroarc foreland basin strata, western North America: Tectonics, v. 32, p. 1027–1048.
Le Bas, M.J., LeMaitre, R.W., Streckeisen, A., and Zanettin, B., 1986, A chemical classification of volcanic rocks based on the total alkali silica diagram: Journal of Petrology, v. 27, p. 745–750.
Le Bas, M.J., and Streckeisen, A.L., 1991, The IUGS systematics of igneous rocks: Journal of the Geological Society of London, v. 148, p. 825–833.
Lonn, J.D., Elliott, C.G., Lewis, R.S., Burmester, R.F., McFadden, M.D., Stanford, L.R., and Jänecke, S.U., 2019, Geologic map of the Montana part of the Salmon 30' x 60' quadrangle, southwestern Montana: Montana Bureau of Mines and Geology Geologic Map 75, 28 p., 1 sheet, scale 1:100,000.
Lowell, W.R., 1965, Geologic map of the Bannack-Grayling area, Beaverhead County, Montana: U.S. Geological Survey Miscellaneous Geologic Investigations Map I-433, scale 1:31,680.
Mosolf, J., in prep.[a], Geologic map of the Dalys 7.5' quadrangle, Beaverhead County, Montana: Montana Bureau of Mines and Geology Geologic Map, 1 sheet, scale 1:24,000.
Mosolf, J., in prep.[b], Geologic map of the Bannack 7.5' quadrangle, Beaverhead County, Montana: Montana Bureau of Mines and Geology Geologic Map, 1 sheet, 1:24,000 scale.
Mueller, P., Mogk, D., and Wooden, J., 2012, Age and composition of crystalline basement in the Armstead anticline, southwestern Montana: Northwest Geology, v. 41, p. 63–70.
Murphy, J.G., 2000, Geochronology of late synkinematic plutons in the Sevier fold and thrust belt, SW Montana: Gainesville, University of Florida, M.S. thesis, 105 p.
Pecora, W.C., 1981, Bedrock geology of the Blacktail Mountains, southwestern Montana: Middletown, Wesleyan University, M.S. thesis, 203 p.
Ruppel, E.T., O'Neill, J.M., and Lopez, D.A., 1993, Geologic map of the Dillon 1º x 2º quadrangle, Idaho and Montana: U.S. Geological Survey Miscellaneous Investigations Series Map I-1803-H, scale 1:250,000.
Schmid, R., Fettes, D., Harte, B., Davis E., Desmons, J. A., 2007, Systematic nomenclature for metamorphic rocks: 1. How to name a metamorphic rock. Recommendations by the IUGS Subcommission on the Systematics of Metamorphic Rocks, https://www.bgs.ac.uk [Accessed June 24th, 2019].
Sears, J.W., 2007, A field guide to middle Miocene karstified erosional surface and debris flows and neotectonic faults near Clark Canyon Reservoir, southwest Montana: Northwest Geology, v. 37, p. 251–260.
Sun, S.S., and McDonough, W.F, 1989, Chemical and isotope systematics of oceanic basalts: Implications for mantle composition and processes, *in* Saunders, A.D., and Norry, M.J., eds., Magmatism in the ocean basins: Geological Society, London, Special Publications, v. 42, p. 313–345.
Tysdal, R.G., 1988, Geologic map along the northeast side of the Blacktail Mountains, Beaverhead County, Montana: U.S. Geological Survey Miscellaneous Field Studies Map MF-2041, scale 1:24:000.
VanDenburg, C.J., Janecke, S.U., and McIntosh, W.C., 1998, Three-dimensional strain produced by >50 My of episodic extension, Horse Prairie basin area, SW Montana, U.S.A.: Journal of Structural Geology, v. 20, p. 1747–1767.
Wardlaw, B.R., and Pecora, W.C., 1985, Mississippian-Pennsylvanian stratigraphic units in southwest Montana and adjacent Idaho: U.S. Geological Survey Bulletin 1656-B, p. B1–B9.
Young, M.L., 1982, Petrology and origin of Archean rocks in the Armstead anticline of southwest Montana: Missoula, University of Montana, M.S. thesis, 64 p.

MBMG
Montana Bureau of Mines and Geology

Geologic Map 81

Geologic Map of the Eli Spring 7.5' Quadrangle, Beaverhead County, Montana

Jesse G. Mosolf

2021